

2004, ApJ, 600, Jan. 10 issue, in press.

The N Enrichment and Supernova Ejection of the Runaway Microquasar LS 5039¹

M. V. McSwain², D. R. Gies³, W. Huang^{3,4}, P. J. Wiita, D. W. Wingert

Center for High Angular Resolution Astronomy

Department of Physics and Astronomy

Georgia State University, University Plaza, Atlanta, GA 30303-3083

*Electronic mail: mcswain@chara.gsu.edu, gies@chara.gsu.edu, huang@chara.gsu.edu,
wiita@chara.gsu.edu, wingert@chara.gsu.edu*

L. Kaper

*Astronomical Institute “Anton Pannekoek”, University of Amsterdam, Kruislaan 403,
NL-1098 SJ Amsterdam, The Netherlands*

Electronic mail: lexk@science.uva.nl

ABSTRACT

We present an investigation of new optical and ultraviolet spectra of the mass donor star in the massive X-ray binary LS 5039. The optical band spectral line strengths indicate that the atmosphere is N-rich and C-poor, and we classify the stellar spectrum as type ON6.5 V((f)). The N-strong and C-weak pattern is also found in the stellar wind P Cygni lines of N V λ 1240 and C IV λ 1550 (narrow absorption components in the former indicate that the wind terminal velocity is $V_\infty = 2440 \pm 190$ km s⁻¹). We suggest that the N-enrichment may result from internal mixing if the O-star was born as a rapid rotator, or the O-star may have accreted N-rich gas prior to a common-envelope interaction with the

²Visiting Astronomer, Cerro Tololo Interamerican Observatory, National Optical Astronomy Observatories, operated by the Association of Universities for Research in Astronomy, Inc., under contract with the National Science Foundation.

³Visiting Astronomer, University of Texas McDonald Observatory.

⁴Visiting Astronomer, Kitt Peak National Observatory, National Optical Astronomy Observatories, operated by the Association of Universities for Research in Astronomy, Inc., under contract with the National Science Foundation.

progenitor of the supernova. We re-evaluated the orbital elements to find an orbital period of $P = 4.4267 \pm 0.0005$ d. We compared the spectral line profiles with new non-LTE, line-blanketed model spectra from Lanz & Hubeny (2003), from which we derive an effective temperature $T_{\text{eff}} = 37.5 \pm 1.7$ kK, gravity $\log g = 4.0 \pm 0.1$, and projected rotational velocity $V \sin i = 140 \pm 8$ km s⁻¹. We fit the UV, optical, and IR flux distribution using a model spectrum and extinction law with parameters $E(B - V) = 1.28 \pm 0.02$ and $R = 3.18 \pm 0.07$. We confirm the co-variability of the observed X-ray flux and stellar wind mass loss rate derived from the H α profile (Reig et al. 2003), which supports the wind accretion scenario for the X-ray production in LS 5039. Wind accretion models indicate that the compact companion has a mass $M_X/M_{\odot} = 1.4 \pm 0.4$, consistent with its identification as a neutron star. We argue that the O-star has a mass in the range $20 - 35M_{\odot}$ (based upon a lower limit for the distance and the lack of eclipses). The observed eccentricity and runaway velocity of the binary can only be reconciled if the neutron star received a modest kick velocity due to a slight asymmetry in the supernova explosion (during which $> 5 M_{\odot}$ was ejected).

Subject headings: binaries: spectroscopic — stars: abundances — stars: early-type — stars: individual (LS 5039, RX J1826.2–1450) — X-rays: binaries

1. Introduction

Massive stars in close binaries are destined to interact in some way over their lifetimes. The initially more massive star is the first to evolve, and after shedding its outer, H-rich envelope by stellar winds, it may begin mass transfer of CNO nuclear processed gas to its companion (de Loore & Vanbeveren 1994). After completion of the mass transfer stage, the abundance ratio of N/C in the photosphere of the gainer may have increased from the solar value of 0.3 to an enriched value of 3 (De Greve & de Loore 1992), or even higher if the mass accretion had induced large scale mixing in the mass gainer (Vanbeveren & de Loore 1994). However, there is conflicting evidence about whether or not mass transfer actually occurs in real binaries composed of massive, O-type stars (Langer et al. 2003). The massive X-ray binaries (MXRBs), for example, generally do not exhibit evidence of N-enrichment, and this

¹Based on observations with the NASA/ESA Hubble Space Telescope obtained at the Space Telescope Science Institute, which is operated by the Association of Universities for Research in Astronomy, Incorporated, under NASA contract NAS5-26555.

fact suggests that the supernova (SN) progenitor may eject mass from the entire system, perhaps during a Luminous Blue Variable stage (Dearborn 1977; Wellstein & Langer 1999).

We were surprised, therefore, to discover that the C IV $\lambda\lambda 5801, 5812$ lines in the spectrum of the MXRB and microquasar LS 5039 (type O6.5 V((f)); Clark et al. (2001)) displayed a weakness indicative of CNO processed gas (McSwain et al. 2001). LS 5039 is also unusual in several other respects. It is one of only a few confirmed MXRBs with associated radio emission (Ribó et al. 1999; Paredes et al. 2002). It has radio-emitting relativistic jets characteristic of galactic microquasars, and it is probably a high energy gamma ray source as well (Paredes et al. 2000). We found that the system is a short period binary with the highest known eccentricity ($e = 0.41 \pm 0.05$) among O star binaries with comparable periods (McSwain et al. 2001). This high eccentricity probably resulted from the huge mass loss that occurred with the SN explosion that gave birth to the compact star in the system (Bhattacharya & van den Heuvel 1991; Nelemans et al. 1999). Binaries that suffer large mass loss in a SN are expected to become runaway stars, and recently both we (McSwain & Gies 2002) and Ribó et al. (2002) found that LS 5039 has a significant proper motion indicating a large peculiar space velocity.

Here we present results from new optical and ultraviolet spectroscopy that confirm the presence of CNO processed gas in the photosphere of LS 5039. We give revised orbital elements for the binary (§2), and we use our combined optical spectra to assign LS 5039 to the category of the N-rich ON stars (§3). We present the first UV spectra of LS 5039 (made with HST/STIS) that we analyze to determine the stellar wind properties (§4) and interstellar reddening (§5). We use the new results to revisit the issue of the masses of the O-star and compact companion (§6). We also present simple models for the change in orbital elements caused by the supernova (§7), which require a modest kick velocity in order to reproduce the observed eccentricity and runaway velocity. Finally we discuss the possible explanations for the N-enrichment given our current understanding of the evolutionary history of the system (§8).

2. Optical Spectroscopy and Orbital Elements

We obtained new spectra of LS 5039 on four different observing runs, and the details about the spectrograph setup in each case are summarized in Table 1. The primary set of blue region spectra come from observations with the University of Texas McDonald Observatory 2.7 m telescope and Large Cassegrain Spectrograph (LCS) on two observing runs (see Gies et al. (2002) for details). All these were made with a TI CCD (800×800 , $15.2 \mu\text{m}$ pixels) except on one night when we used a Loral/Fairchild CCD (1024×1024 , $12 \mu\text{m}$ pixels).

Most of the spectra were made in a single 1200 s exposure that resulted in a signal-to-noise ratio of $S/N = 120$ in the continuum. A secondary set of blue spectra were made with the CTIO 1.5 m telescope and Cassegrain spectrograph (CS) using a Loral CCD (1024×1024 , $15 \mu\text{m}$ pixels). These were usually 1800 s exposures that produced a $S/N = 80$ in the continuum. We also observed the red spectral region during a KPNO Coude Feed run in 2002 June. These spectra are comparable to those we presented in McSwain et al. (2001) except that these new spectra were obtained with a TI CCD that had smaller wavelength coverage. Finally, we obtained one additional red spectrum of lower resolving power with the CTIO 1.5 m CS on 2003 March 21. All these spectra were extracted and calibrated using standard techniques in IRAF⁵. We removed atmospheric telluric lines from the red spectra using spectra of broad-lined A-type stars (see McSwain et al. (2001)).

Our first task was to re-evaluate the orbital elements presented in McSwain et al. (2001) using an enlarged set of radial velocity measurements. We measured radial velocities for the blue spectra by cross-correlating each spectrum with the average of the blue spectra made at McDonald Observatory (the largest homogeneous set). We omitted spectral regions containing interstellar features. These relative velocities were converted to an absolute scale by adding the radial velocity of the average spectrum as determined by parabolic fitting of the cores of the strong lines, $+11.2 \pm 9.2 \text{ km s}^{-1}$ (using rest wavelengths from Bolton & Rogers (1978)). Radial velocities from the red spectra were also determined by cross-correlation techniques, but in this case the reference spectrum was formed by a shift-and-add average of the red spectra obtained earlier (McSwain et al. 2001). This cross-correlation function is generally based on the positions of the $\text{H}\alpha$ and $\text{He I } \lambda 6678$ features, but for the CTIO red spectrum we also included the spectral regions containing $\text{He I } \lambda 5876$ and $\text{He II } \lambda 6527$. We also determined the cross-correlation positions of the sharp interstellar line at 6614 \AA that we used to make small velocity corrections between observatories. The 14 new radial velocity measurements are collected in Table 2.

Our first attempt to revise the orbital period and other elements starting with the period we found earlier ($P = 4.117 \text{ d}$; McSwain et al. (2001)) failed, with 8 of the 14 new measurements falling far from the calculated radial velocity curve. Thus, we made a new period search using the discrete Fourier transform method of Roberts et al. (1987). There are a number of candidate peaks in the periodogram that are clustered around a frequency of $0.25 \text{ cycles d}^{-1}$, and most of these are aliases introduced by our sparse data sampling (McSwain et al. 2001). We tested each of these candidate periods using the nonlinear, least-

⁵IRAF is distributed by the National Optical Astronomy Observatories, which is operated by the Association of Universities for Research in Astronomy, Inc., under cooperative agreement with the National Science Foundation.

squares fitting program of Morbey & Brosterhus (1974) to determine the orbital elements, and only one of the test periods, $P = 4.4267 \pm 0.0005$ d, led to consistent placement of all the new measurements. This value was also the primary signal found using the Phase Dispersion Minimization technique of Stellingwerf (1978) that is useful for finding periodicities in non-sinusoidal variations. Significantly, this period also fits new radial velocity data obtained by J. Casares, M. Ribó, J. M. Paredes, and J. Martí (in preparation). The revised orbital elements are given in Table 3, and the observations and radial velocity curve are shown in Figure 1. This fit assumed equal weights for each radial velocity measurement; fits weighted using the inverse square of the standard deviation of each measurement led to identical results within errors. Aside from the orbital period, the new elements do not differ greatly from those we presented earlier (McSwain et al. 2001). Most of our observations are clustered into runs of a week or so (comparable to the period) so that while the placement of these groups of measurements in phase is somewhat altered, the overall shape of the curve is much the same.

3. Spectral Classification and Stellar Parameters

Clark et al. (2001) discuss the appearance of the optical and near-IR spectrum of LS 5039, from which they derive a spectral classification of O6.5 V((f)) for the mass donor star. Here we examine the line patterns in our optical spectra to confirm this classification. We formed an average blue spectrum by calculating a shift-and-add mean spectrum from our McDonald and best CTIO spectra (based upon the line shifts from the orbital solution in the last section). The average interstellar spectrum was divided out of each observed spectrum prior to forming the average. The resulting mean spectrum is shown in the upper plot in Figure 2 together with identifications for the more prominent lines. We also show in this diagram the blue spectra of the standard stars HD 93146 (O6.5 V((f)); from the atlas of Walborn & Fitzpatrick (1990)) and 15 Mon (O7 V((f)); obtained during our CTIO run). Lanz & Hubeny (2003) have recently made available a library of synthetic stellar spectra for a grid of non-LTE atmospheres appropriate for O-type stars⁶, and we show in Figure 2 a flux rectified version of one of their models (with stellar parameters discussed below). This spectrum was convolved with broadening functions to simulate stellar rotational and spectrographic instrumental broadening (discussed below).

The spectral subtype among O-type stars is defined by the relative strengths of the He II and He I lines (Walborn & Fitzpatrick 1990). The relative strengths of the He II

⁶<http://tlusty.gsfc.nasa.gov>

$\lambda 4541$ and He I $\lambda 4471$ lines in the spectrum of LS 5039 make a good match with the O6.5 V((f)) standard star (but not with the cooler O7 V((f)) spectrum in which He I $\lambda 4471$ is stronger). The primary luminosity criterion at this spectral type is the strength of the He II $\lambda 4686$ line that ranges from strong absorption to strong emission between main sequence and luminous supergiant stars (see Fig. 9 in Walborn & Fitzpatrick (1990)). The deep He II $\lambda 4686$ absorption line in the spectrum of LS 5039 clearly indicates a luminosity class V object. We also observe weak emission in the N III $\lambda\lambda 4634 - 4640 - 4642$ blend, which is indicated by the classification suffix ((f)). Our results therefore confirm the spectral classification obtained by Clark et al. (2001) of O6.5 V((f)).

We note, however, the unusual strength of the N III $\lambda 4379$ and N III $\lambda 4510 - 4514 - 4518$ features in the spectrum of LS 5039 compared to the other reference spectra. These lines tend to peak near type O8.5, and at any given subtype they increase in strength with luminosity (Mathys 1989). The equivalent width of the N III $\lambda 4510 - 4514 - 4518$ blend in the spectrum of LS 5039 is $W_\lambda = 0.40 \pm 0.04 \text{ \AA}$, which is larger than that in all 13 N-strong stars with spectral types O7 or earlier listed by Mathys (1989) (with the exception of the N enhanced, O7 V((f)) star, HD 90273). Furthermore, we observe that the C III $\lambda 4650$ blend is weak or absent in the spectrum of LS 5039, and other C features are also unusually weak (C III $\lambda 4187$, C III $\lambda 5696$ emission, C IV $\lambda 5801, 5812$). We show below that this trend of strong N and weak C is also found in the UV stellar wind lines (§5). These characteristics are the hallmark of the ON type stars that appear to be contaminated with CNO nuclear processed gas (Walborn 1976; Bolton & Rogers 1978; Schönberner et al. 1988; Mathys 1989). One of the hottest stars that is currently assigned to the ON group is HD 110360 (ON7 V; Mathys (1989)), and the strong similarity in appearance between LS 5039 and HD 110360 (see Fig. 5 in Mathys (1989)) suggests that LS 5039 also belongs to this group. Thus, we advocate a classification of ON6.5 V((f)) for the spectrum of LS 5039.

The appearance of the optical line spectrum can also be used to help estimate the physical properties of the star using the new non-LTE model spectra from Lanz & Hubeny (2003). A direct comparison of their grid of model spectra with our observed spectrum can provide reliable estimates of the stellar projected rotational velocity $V \sin i$, the effective temperature T_{eff} , and the gravitational acceleration $\log g$. We adopted the Lanz & Hubeny (2003) solar metallicity models, which assume an atmospheric microturbulent velocity of 10 km s^{-1} . We used our relatively higher dispersion red spectra ($\lambda/\Delta\lambda = 3510$; McSwain et al. (2001)) to find a value of $V \sin i$ that would produce a match of the model and observed profiles of the strong He I $\lambda 5876$ line. We formed a rotational broadening function for a linear limb darkening law (Gray 1992) using a limb darkening coefficient from the tables of Wade & Rucinski (1985), and then the Lanz & Hubeny (2003) model spectrum was convolved with this and a Gaussian instrumental broadening function for direct comparison with the

observed profile. The best fit was made with $V \sin i = 140 \pm 8 \text{ km s}^{-1}$, which is in good agreement with our earlier result of $V \sin i = 131 \pm 6 \text{ km s}^{-1}$ based upon the half-width of the O III $\lambda 5592$ line (McSwain et al. 2001).

We estimated the effective temperature by comparing the observed He II to He I line ratios with those predicted from the grid of model spectra from Lanz & Hubeny (2003). We measured equivalent widths of the major He lines by Gaussian fitting of the observed spectral profiles, and we then formed logarithms of the important ratios used in spectral classification (Table 4). We made numerical integrations across the same lines in the grid of model spectra by Lanz & Hubeny (2003) and then formed plots of $\log[W_\lambda(\text{He II})/W_\lambda(\text{He I})]$ versus T_{eff} . We restricted the grid to models with $\log g = 4.0$, which is the appropriate gravity for main sequence stars (see below). Table 4 lists the resulting values of T_{eff} made by interpolation with the observed ratios in these curves. We formed a final mean temperature by double weighting the result from the primary ratio that defines the classification sequence, He II $\lambda 4541$ to He I $\lambda 4471$, to arrive at $T_{\text{eff}} = 37.5 \pm 1.7 \text{ kK}$. This temperature is somewhat low for spectral type – temperature calibrations based upon pure H and He model atmospheres (Vacca et al. 1996) but it agrees well with more recent calibrations that rely on blanketed, non-LTE models (Martins et al. 2002).

The stellar gravity, $\log g$, is presumably the key parameter defining the appearance of the He II $\lambda 4686$ line for stars of this temperature (Walborn & Fitzpatrick 1990). However, the emergence of this feature as an emission line in more luminous stars is the result of their vigorous stellar winds, and unfortunately the Lanz & Hubeny (2003) models are based on static, plane parallel atmospheres that will not predict the He II $\lambda 4686$ line strength correctly in most cases. Instead, we can use the Stark broadening of the H Balmer lines to help estimate the atmospheric pressure and hence gravity. $H\gamma$ is the most suitable feature in our spectra for this purpose since $H\delta$ is severely blended with N III $\lambda 4097$ at this spectral resolution. We show in Figure 3 the observed and model $H\gamma$ profiles for $\log g = 3.7, 4.0$, and 4.3 (cgs units). These model profiles were convolved with both the rotational and instrumental broadening functions. The comparison indicates that $\log g = 4.0 \pm 0.1$. However, we caution that this value may be biased upwards by the presence of N III lines in the wings of $H\gamma$ (wavelengths from the NIST database⁷) that are probably underestimated by the Lanz & Hubeny (2003) models in this particular case.

A reliable abundance analysis is clearly desirable, but will require higher dispersion spectra to account for the effects of line blending in the vicinity of the key CNO lines. However, we made preliminary estimates by calculating line profiles for a range of assumed

⁷<http://physics.nist.gov/cgi-bin/AtData/main.asd>

abundances using the radiative transfer code *Synspec* and the non-LTE stellar atmosphere associated with our derived values of T_{eff} and $\log g$ (Lanz & Hubeny 2003). We found that the equivalent width of the N III $\lambda\lambda 4510, 4514, 4518$ blend ($W_{\lambda} = 0.40 \pm 0.04 \text{ \AA}$) corresponds to a N abundance of $+0.68 \pm 0.09$ dex relative to the solar value. The equivalent width of C III $\lambda 4187$ ($W_{\lambda} = 0.03 \pm 0.01 \text{ \AA}$) yields a C abundance of -0.55 ± 0.20 dex (i.e., sub-solar). These trends are consistent with our expectations for CNO processed gas (Schönberner et al. 1988).

4. HST/STIS Spectroscopy and UV Wind Lines

The ultraviolet spectra of O-type stars are a key source of information about their photospheres and stellar winds (Walborn et al. 1985), and we were fortunate to obtain the first ever UV spectra of LS 5039 with the *Hubble Space Telescope* Space Telescope Imaging Spectrograph (STIS) in 2002 August. During the first visit to the target (2002 Aug 13) we obtained two exposures (exposure times of 2087 and 1814 s) with the G140L grating and one exposure (600 s) with the G230L grating. The G140L grating covers the wavelength range $1150 - 1730 \text{ \AA}$ with a resolving power of $\lambda/\Delta\lambda = 1000$ while the G230L grating records the range $1570 - 3180 \text{ \AA}$ with a resolving power of $\lambda/\Delta\lambda = 500$. A second visit was made 7 days later (2002 Aug 20) to obtain a single exposure (2087 s) with the G140L grating. These visits correspond to orbital phases 0.145 and 0.708, respectively, when the O-star primary was oriented at an angle from the line of the nodes in the orbital plane of $\nu + \omega = 16^\circ$ and 121° , respectively (§2). Thus, the first visit occurred just past the quadrature phase when the orbital axis was orthogonal to our line of sight and the second visit was made shortly after primary superior conjunction (compact companion in the foreground). There were no obvious flux or profile variations between these visits, so we formed an exposure weighted average FUV spectrum for examination.

We obtained a single UV spectrum from the archives of the *International Ultraviolet Explorer Satellite*⁸ of the same O6.5 V((f)) reference standard shown above in Figure 2, HD 93146, to compare to that of LS 5039. We rebinned the high dispersion *IUE* spectrum (SWP 11136) of HD 93146 onto the wavelength grid of the STIS FUV spectrum, and both the reference and target spectra were rectified to a pseudo-continuum by division of a polynomial fit made through relatively line-free regions. Two sections of these spectra in the immediate vicinity of the strong stellar wind lines N V $\lambda 1240$ and C IV $\lambda 1550$ are illustrated in Figures 4 and 5, respectively. There is generally good agreement between the spectra of LS 5039 and

⁸<http://archive.stsci.edu/iue>

HD 93146 in the UV photospheric lines. There are differences, however, in the interstellar line strengths and especially in the wind lines. We find that the N V $\lambda 1240$ P Cygni profile has both a deeper blue absorption component (due to stellar wind material projected against the disk of the star) and a stronger red emission component (from scattered light surrounding the star) than is seen in the spectrum of HD 93146. The differences occur in the opposite sense in the C IV $\lambda 1550$ wind profile. The enhanced N and weak C features mirror the results found in the optical spectra, and these same wind line differences are found in other ON type stars (Walborn et al. 1985, 2000).

Both wind profiles have shapes that are similar to their counterparts in the spectrum of HD 93146, and in particular, there are two minima in the absorption part of the N V $\lambda 1240$ feature in the spectra of both stars. These minima appear much narrower in the high dispersion version of the HD 93146 spectrum, and their spacing corresponds to the highly blueshifted positions of the N V doublet. They are examples of narrow (or discrete) absorption components (NAC) that often appear in the UV wind lines (Prinja et al. 1990; Kaper et al. 1999). Detailed time sequences demonstrate that NAC usually proceed blueward through the trough and become narrower. Prinja et al. (1990) show that the sum $v_{\text{NAC}} + \text{HWHM}_{\text{NAC}}$ is approximately constant and equal to the extreme velocity found in saturated line cores, and they argue that this quantity is a good estimate of the wind terminal velocity, v_∞ . We measured the Doppler shifts of both minima in the N V $\lambda 1240$ profile of LS 5039, and we find $v_{\text{NAC}} = 2270 \pm 100 \text{ km s}^{-1}$. The resolving power of the STIS spectra is too low to determine the NAC width, so we assumed it is the same as Prinja et al. (1990) found for HD 93146, $\text{HWHM}_{\text{NAC}} = 165 \text{ km s}^{-1}$. Thus, we estimate that the wind terminal velocity for LS 5039 is $V_\infty = 2440 \pm 190 \text{ km s}^{-1}$, which agrees well with the mean for the O6.5 V subtype of $V_\infty = 2455 \text{ km s}^{-1}$ (Prinja et al. 1990).

In some MXRBs these wind lines display orbital phase variations due to excess ionization of the wind in a zone surrounding the X-ray source (the *Hatchett-McCray effect*; Hatchett & McCray (1977); van Loon et al. (2001)). The wind profiles of LS 5039 that we observed with HST/STIS showed no evidence of changes between the quadrature and superior conjunction phases. The X-ray flux was moderately low at the time of the observations (see Fig. 7 below). If the X-ray source ionized a large volume that included regions projected against the stellar disk in the superior conjunction phase, then portions of the blue absorption trough would weaken as the scattering ions are ionized to higher levels (van Loon et al. 2001). However, we suspect that the ionized region is small compared to the system dimensions in the case of LS 5039. van Loon et al. (2001) use the same wind accretion model we discuss in §6 to show that the q parameter defining the extent of the ionization zone scales as $a^2 v_{\text{vel}}^3$ among MXRBs, where a is the separation of the components and v_{vel} is the wind velocity relative to the neutron star. For the separation at the time of the *HST* near superior conjunction

observation, we estimate that this parameter falls in the range $q \approx 500 - 800$, based upon a comparison with results for Vela X-1 from van Loon et al. (2001). This corresponds to a Strömgren sphere radius of approximately 4% of the system separation (see eq. [4] in van Loon et al. (2001)). The minimum projected separation between the outer edge of the ionization sphere and stellar limb at the observed phase is approximately $1.5R_O$ (for an inclination $i = 90^\circ$), so that no occultation is expected. We suspect that any wind profile variations will be restricted to phases very close to superior conjunction and will only be observed if the system has a relatively large orbital inclination (§6).

5. Reddening and Extinction

The reddening and extinction of LS 5039 are directly related to the issues of the star’s distance and space velocity (§6). Clark et al. (2001) and Ribó et al. (2002) both argue that the reddening is $E(B - V) = 1.2 \pm 0.1$, and Ribó et al. (2002) suggest that the distance is $d = 2.9 \pm 0.3$ kpc based upon an assumed absolute magnitude. The flux in the UV spectral range is very sensitive to the extinction curve (Fitzpatrick 1999), so we decided to re-investigate the reddening using the new STIS spectra. The STIS spectra are shown in Figure 6 in a version rebinned to a resolving power of $\lambda/\Delta\lambda = 100$. We have included in Figure 6 fluxes based upon Johnson-Cousins and near-IR photometry from Clark et al. (2001) and the 2MASS survey (Cutri et al. 2003), plus new Strömgren u, v, b , and y measurements we made on 2002 June 24 using the CTIO 0.9 m telescope and SITE 2048 \times 2048 CCD. We also observed six standard stars (HD 105498, HD 128726, HD 156623, HD 157795, HD 167321, and HD 216743), taken from lists by Cousins (1987) and Clausen et al. (1997), in each band at a minimum of three different airmasses each to calibrate the photometry. All of the instrumental magnitudes were determined using a large aperture of 8 arcsec, and the photometric transformation equations from Henden & Kaichuck (1982) were applied to determine the apparent magnitudes of LS 5039: $u = 13.25 \pm 0.05$, $v = 12.72 \pm 0.04$, $b = 12.10 \pm 0.02$, and $y = 11.31 \pm 0.02$. The errors in the magnitudes are from the combined estimated instrumental errors and the errors in the transformation constants.

The IR measurements were transformed to fluxes using the NICMOS units conversion tool⁹. We determined fluxes from the optical band photometry using the IRAF routine *calcphot* in the *HST stsdas/synphot* package. This was done by comparing the difference in calculated magnitude between a reddened model spectrum of LS 5039 (a preliminary version of that discussed below) and a spectrum of Vega with the observed difference in

⁹http://www.stsci.edu/hst/nicmos/tools/conversion_form.html

magnitude (using Vega magnitudes from Bessell (1983) and Gray (1998)). The model fluxes at the central filter wavelengths were then prorated to match the calculated and observed magnitude differences.

We assumed that the model fluxes from Lanz & Hubeny (2003) for the spectroscopically determined parameters $T_{\text{eff}} = 37.5$ kK and $\log g = 4.0$ provided a reliable estimate of the spectral flux distribution at the stellar photosphere. We then calculated how the observed spectrum at Earth appears based upon the interstellar reddening curve given by Fitzpatrick (1999). There are three parameters that determine the appearance of the transformed spectrum: the reddening, $E(B - V)$, the ratio of total to selective extinction at V , $R = A(V)/E(B - V)$, and the ratio of stellar radius to distance, R_O/d (equivalent to half the angular diameter in radians). The first two parameters determine the shape of the extinction curve, while the final parameter is a normalization factor. We formed χ^2 residuals for a grid of $E(B - V)$ and R values to find the best fit values that minimized χ^2 . The best fit, shown by the solid line in Figure 6, was made with $E(B - V) = 1.28 \pm 0.02$, $R = 3.18 \pm 0.07$, and $R_O/d = (8.2 \pm 0.6) \times 10^{-11}$ (angular diameter = 0.03 mas). This transformed spectrum fits well the entire FUV to IR range. We also show 1σ deviations from this fit in $E(B - V)$ (*dotted line*) and in R (*dashed line*).

There are two nearby stars along the line of sight to LS 5039 that have comparable extinction: BD-14°5043 (B1 IV) with $A_V = 3.73$ and $d = 1.1$ kpc (Kilkenny 1993; He et al. 1995) and BD-14°5040 (O8 V) with $A_V = 4.00$ and $d = 1.9$ kpc (Kilkenny 1993). Our derived extinction of $A_V = 4.2 \pm 0.2$ indicates that the distance to LS 5039 is greater than 1.9 kpc, which is consistent with prior estimates ($d = 2.9 \pm 0.3$ kpc; Ribó et al. (2002)).

6. Masses

In our previous paper (McSwain & Gies 2002), we estimated the probable secondary mass for a range in primary mass by comparing the observed and predicted X-ray fluxes for wind accretion. Here we re-consider those arguments in light of the new results given above. The independent parameter is the mass of the O star, M_O , that sets many of the other stellar parameters. The gravity determination from §3, $\log g = 4.0 \pm 0.1$, establishes the relationship between mass and radius, $\log g_{\text{eff}} = (1 - \Gamma)GM/R^2$, where the ratio of radiative acceleration by electron scattering to gravitational acceleration is $\Gamma = 2.6 \times 10^{-5}(L/L_\odot)/(M/M_\odot)$. The specific relationship for LS 5039 based upon the derived effective temperature (§3) is $R_O/R_\odot = (1.56 \pm 0.16)(M_O/M_\odot)^{1/2}$. The fit of the observed flux distribution yields the angular diameter (§5), which leads to a distance estimate of $d = (0.28 \pm 0.02)R_O/R_\odot$ kpc (somewhat closer than our prior estimate of $d = 0.32R_O/R_\odot$ kpc; McSwain & Gies (2002)).

We estimate the wind mass loss rate using the equivalent width of the H α emission line and the method of Puls et al. (1996). The H α profile appears as a deep absorption line in stars with minimal wind, and the feature becomes progressively filled-in as the mass loss rate increases (appearing as a pure emission line in stars with strong winds). The mass loss rate depends upon the net emission equivalent width (i.e., the difference between the observed and purely photospheric absorption equivalent widths), the choice of the wind velocity law exponent β , the wind terminal velocity v_∞ , and the stellar effective temperature (Puls et al. 1996). We revised our assumptions about several of these parameters. We adopted $T_{\text{eff}} = 37.5$ kK (§3) and used the detailed optical flux model from Lanz & Hubeny (2003) to find the appropriate photospheric equivalent width for H α , $W_\lambda = 3.27$ Å. We adopted a velocity law index of $\beta = 1.0$ that Puls et al. (1996) advocate as the appropriate value for the weak wind case we find here. Finally, we set the terminal velocity to $V_\infty = 2440$ km s $^{-1}$, the value we estimated from the wind profiles in the STIS spectra (§4). Most of these changes result in a moderate decrease in the estimated mass loss rate (Table 5, row 3) compared to our earlier results (McSwain & Gies 2002).

We noted in the previous paper that the H α strength appears to be variable on time-scales longer than our observing runs (McSwain & Gies 2002), which implies that there are long term variations in the mass loss rate. Reig et al. (2003) have recently shown that there are also long term variations in the X-ray flux that appear to be related to those observed in H α . We show in Figure 7 the time evolution of the X-ray flux in the 0.3 – 10 keV range reported by Reig et al. (2003). Figure 7 also illustrates the mass loss rate variations determined from the H α equivalent widths from McSwain & Gies (2002) (3 measurements), Reig et al. (2003) (2 measurements), and our two recent observations ($W_\lambda = 2.83$ Å and 2.95 Å for 2002 June 25 and 2003 March 21, respectively). The y -axes in Figure 7 were scaled to overlap the X-ray flux and mass loss estimates as closely as possible, and we confirm that these two quantities appear to vary in concert in the limited data available. This result supports the wind accretion model and the validity of the mass loss estimates. It also points out the need to compare the predicted and observed accretion luminosities at an epoch when nearly simultaneous optical and X-ray data are available. Here we will make the comparison for the closely spaced KPNO Coude Feed (McSwain & Gies 2002) and BeppoSAX (Reig et al. 2003) observations made in 2000 October, which correspond to a mass loss rate and X-ray flux minimum in Figure 7.

We calculated the predicted wind accretion X-ray luminosity for a given M_O and a grid of companion masses M_X using the method of Lamers et al. (1976), and then we determined which M_X value produced an X-ray luminosity that matched the observed value. This procedure was essentially the same as described earlier (McSwain & Gies 2002), but we improved our accretion rate estimate by finding the mean of rates for equal time samplings

around the elliptical orbit and by adopting the observed projected rotational velocity (§3) in the calculation of the wind – companion relative velocity (see eq. [7b] in Lamers et al. (1976)). The resulting best-fit masses are listed in Table 5 and are illustrated in a mass plane diagram in Figure 8. Note that the stellar radius is well within its critical Roche radius at periastron in all these models, so that mass accretion by Roche lobe overflow is probably not a significant process in LS 5039. Our revised M_X estimates are smaller than but comparable to what we found previously (see Fig. 2 in McSwain & Gies (2002)). The main reason for this difference is that we relied in the earlier paper on an X-ray luminosity estimate that turned out to be a local maximum (the first point shown in Fig. 7), and this consequently required a larger M_X to account for the accretion luminosity.

The lightly shaded region surrounding the best-fit mass estimates in Figure 8 shows how the solutions vary with changes in assumed parameters. The lower envelope corresponds to the calculations made using a wind velocity law exponent $\beta = 0.8$ instead of the 1.0 value recommended by Puls et al. (1996). A lower exponent corresponds to a higher mass loss estimate (see Fig. 15 in Puls et al. (1996)), and this must be balanced by a lower mass accretor in order to match the observed X-ray luminosity (see eq. [21] in Lamers et al. (1976)). The upper envelope shows the results obtained by assuming that the H α equivalent width was 1σ larger ($W_\lambda = 3.20$ Å) than actually observed in 2000 October ($W_\lambda = 3.10$ Å). The increased equivalent width corresponds to a weaker stellar wind (less emission), and in fact the assumed value is close to that for no wind ($W_\lambda = 3.27$ Å). Here a reduction in wind strength is compensated by an increase in accretor mass in order to maintain the observed X-ray luminosity. These tests indicate that our estimates for M_X based upon the accretion model have formal errors of approximately $\pm 0.4M_\odot$. However, we caution that the actual errors may be larger because the simple wind accretion model does not account for the effects of the ionization of the wind by the X-ray source and because the efficiency parameter for conversion of accreted matter into X-ray radiation, ζ , is only known approximately. Nevertheless, our results for M_X are consistent with a neutron star companion.

There are several considerations that can help limit the range of acceptable mass for the O-star. The observed reddening of LS 5039 compared to nearby, line-of-sight stars indicates a minimum distance of 1.9 kpc (§5), and this distance corresponds to a lower limit on the stellar mass of $M_O > 20M_\odot$. The wind accretion solutions at the high mass end require increased mass loss rates and larger system dimensions; such combinations occur at high inclinations according to the orbital mass function. The dashed line in Figure 8 indicates the inclinations at which eclipses would begin to occur, and we see that for large M_O the best-fit accretion models predict that eclipses should be observed. However, there is no evidence of either X-ray (Ribó et al. 1999; Reig et al. 2003) or optical (Clark et al. 2001) eclipses despite significant efforts to find them. Thus, the probable absence of eclipses and

the results of the wind accretion model suggest an upper mass limit of approximately $35M_{\odot}$ (although masses as large as $50M_{\odot}$ still fall within the error zone of the wind accretion model results).

The wind properties offer additional constraints on the O-star mass. Hot massive stars have a wind momentum product, $\dot{M} v_{\infty} R_{\star}^{0.5}$, that is directly related to the stellar luminosity (Kudritzki & Puls 2000), and rows 3 and 4 of Table 5 compare our $\text{H}\alpha$ derived mass loss rate with that predicted by the empirical wind momentum relationship for Galactic O-stars. The agreement appears best at the low mass end, but there is ± 1.2 dex scatter in the wind momentum product among the stars that define the empirical relationship, so the full $20 - 40M_{\odot}$ range remains viable. Table 5 also lists the ratio $v_{\infty}/v_{\text{esc}}$, which typically has a value of 2.6 in O-type stars (Lamers & Cassinelli 1999). This criterion would again favor the lower mass range for LS 5039, $M_O \approx 20M_{\odot}$, but we caution that there is a large spread in this ratio among hot stars. Indeed, Prinja et al. (1990) find a ratio $v_{\infty}/v_{\text{esc}} = 1.7$ for the comparable ON8 V star, HD 14633, and van Loon et al. (2001) quote ratio estimates in the range 0.8 – 2.8 in other MXRBs.

The final row of Table 5 gives estimates of the equatorial velocity V_{eq} that are derived from the projected rotational velocity assuming that the spin axis is aligned with the orbital axis (see Table 6 below) and that the orbital inclination can be set from the wind accretion models.

7. Pre-Supernova Orbital Parameters

The eccentricity of the system probably results from the supernova event that formed the neutron star, and the current value of the eccentricity can be used to infer the pre-SN orbital parameters, assuming that no asymmetrical kick velocity was imparted to the neutron star during the explosion and that the eccentricity has not decreased since the SN (McSwain & Gies 2002; Ribó et al. 2002). We show in the top portion of Table 6 estimates of the pre-SN orbital period, P^{initial} , and mass of the SN-progenitor just prior to the SN, M_2^{initial} , based upon the current orbital elements, mass solutions from the wind accretion model, and the assumption of $v_{\text{kick}} = 0$. There are several problems with these models that result from our revisions to the distance and eccentricity compared to earlier work (McSwain & Gies 2002). The paramount difficulty is the apparent discrepancy between the runaway velocity expected from the eccentricity and masses, v_{sys} (predicted), and the peculiar space velocity, v_{pec} (derived) (based upon the observed proper motion and radial velocity, the distance associated with a given stellar mass M_O , and the method described in Berger & Gies (2001)). The former is approximately twice as large as the latter, a much

greater difference than expected from their formal errors (approximately 14% and 19%, respectively). The second problem is that the predicted pre-SN orbital period is so short that the Roche radius of the O-star is smaller than or equal to the estimated stellar radius. A third, potential, difficulty is the relatively large mass of the SN-progenitor compared to theoretical expectations (Wellstein & Langer 1999).

All of these problems can be alleviated by removing the assumption that the SN kick velocity was zero. There is now a significant body of evidence that non-zero kick velocities must occur in SN (Brandt & Podsiadlowski 1995; van den Heuvel & van Paradijs 1997; Hughes & Bailes 1999; Pfahl et al. 2002). The introduction of a SN kick velocity will dramatically influence the post-SN orbital parameters and system runaway velocity. Following the development of Brandt & Podsiadlowski (1995), we can express the final outcome parameters in terms of two ratios,

$$m = \frac{M_2^{\text{initial}} + M_O}{M_X + M_O}$$

and

$$v = \frac{v_{\text{kick}}}{v_{\text{orb}}},$$

where v_{kick} and v_{orb} are the values of the kick velocity and pre-SN relative orbital velocity, respectively. We also need to specify the direction of the kick in terms of ϕ , the angle between the SN-progenitor’s orbital motion and the kick-velocity vector projected onto the pre-SN orbital plane, and θ , the angle between the kick direction and the pre-SN orbital plane (see Fig. 1 in Brandt & Podsiadlowski (1995)). With these four parameters selected we can determine the post-SN eccentricity, system runaway velocity, and angle ν of misalignment between the O-star rotation axis and the current orbital angular momentum vector (see eq. [2.8, 2.10, 2.16] in Brandt & Podsiadlowski (1995)).

We explored the possible solutions applicable to LS 5039 by calculating the predicted final eccentricity and runaway velocity over a grid of m , v , ϕ , and θ . Our strategy was to compute e and v_{sys} for each set of parameters, and if the results in both cases were within 1σ of the observed values, then we saved the increment of solid angle corresponding to the test values of ϕ and θ in our grid. We omitted any models that led to a pre-SN orbit with an O-star Roche radius smaller than the observed value and any kick directions that would have the SN-remnant strike the O-star. Our final results are shown in Figure 9 for the masses associated with our $M_O = 30M_\odot$ wind accretion model. The grayscale intensity in this figure is directly proportional to the integrated solid angle of acceptable solutions for given values of m and v , so that the figure may be interpreted as a geometrical probability estimate (white corresponding to no solutions possible, black corresponding to the maximum integrated solid angle of acceptable solutions in the (m, v) grid). The high frequency “ripples” in the image

result from the coarseness of our angular grid (increments of 5° in ϕ and θ) and our hard boundaries of $\pm 1\sigma$ for acceptable solutions.

There is a broad range of solutions in the (m, v) plane, but the geometrically favored solutions are concentrated in two regions. The first occurs along a ridge in the lower portion of the diagram near $m = 1.29$ and $v = 0.08$. The solutions correspond to kicks in the direction $\phi = 0^\circ - 55^\circ$, i.e., in approximately the same direction as the orbital motion of the progenitor at the time of the SN. The pre-SN orbital parameters for such prograde ($v_{\text{kick}+}$) solutions are given in the middle portion of Table 6, which lists the solid angle weighted average values of initial period, kick velocity, and misalignment. We find initial periods similar to the no kick case but the progenitor masses are lower. The associated kick velocities are small and consistent with the low values found by Hughes & Bailes (1999) and by Pfahl et al. (2002) for other MXRBs. Pfahl et al. (2002) suggest that small kick velocities may occur in close binaries in which the SN-progenitor was a rapid rotator at the time of the SN (i.e., in those which avoided spin down in a red-supergiant phase). The other geometrically favored region occurs near $m = 1.32$ and $v = 0.46$, and these solutions correspond to retrograde kicks ($v_{\text{kick}-}$) with $\phi = 95^\circ - 180^\circ$. The lower portion of Table 6 gives the pre-SN orbital parameters for such solutions that have a longer initial period (and larger Roche radii) than the other solutions. The kick velocities are much larger than before, but still within the range considered reasonable in other investigations (Brandt & Podsiadlowski 1995). However, the largest kick velocities permitted in Figure 9 (for $v_{\text{kick}} \approx 1400 \text{ km s}^{-1}$ and $\nu > 90^\circ$) are probably too extreme for most of the commonly accepted kick velocity distributions.

We expect that the binary probably suffered a significant reduction in orbital period during a spiral-in, common envelope phase prior to the SN explosion (Taam & Sandquist 2000). At the conclusion of this stage the stars were in a short period orbit, and the strong tidal forces would ensure quick spin synchronization and circularization of the orbit (Zahn 1977; Claret & Cunha 1997). We can estimate the average synchronous rotation speed prior to the SN, $\langle V_{\text{sync}} \rangle$, using R_O (Table 5) and $\langle P^{\text{initial}} \rangle$ (Table 6), and we list these estimates for the $v_{\text{kick}+}$ and $v_{\text{kick}-}$ cases in Table 6. The synchronous rotation speeds are smaller than the observed value of projected rotational velocity ($V \sin i = 140 \pm 8 \text{ km s}^{-1}$) for the $v_{\text{kick}-}$ models, so we prefer the solutions for the $v_{\text{kick}+}$ models. The SN progenitor may also have been a rapid rotator as a result of tidal synchronization, and the lower kick velocities associated with the $v_{\text{kick}+}$ models are consistent with the suggestion that smaller kicks occur in rapid rotators (Pfahl et al. 2002). However, regardless of the choice of the model for the SN event in LS 5039, it is clear that a modest, non-zero kick velocity is required to explain consistently the observed eccentricity and runaway velocity.

8. The Origin of the N Enrichment

It is somewhat surprising that we find clear evidence of CNO processed gas in the photosphere of LS 5039 while the spectral signature of CNO processed gas is generally absent in other MXRBs (with the interesting exceptions of Vela X-1 = HD 77581 (Kaper et al. 1993) and 4U1700–37 = HD 153919 (Clark et al. 2002)). The N-enriched gas has two possible sources, nuclear processed gas from the interior of the O-star and/or processed gas from the envelope of the neutron star progenitor. Here we briefly discuss the issues associated with both sources of enriched gas.

The origin of the He and N enrichment in the OBN and other evolved massive stars is probably related to rotationally induced mixing of the stellar interiors. Heger & Langer (2000) and Meynet & Maeder (2000) have constructed stellar models that include rotation, and they find that significant mixing of CNO processed gas into the photosphere can occur over a main sequence lifetime in rapidly rotating, massive stars. Howarth & Smith (2001) found that the OBN stars have a projected rotational velocity distribution consistent with the assumption that they represent a class of rapid rotators, and they showed that He is enhanced in several very rapidly rotating O-type stars.

The projected rotational velocity of LS 5039 ($V \sin i = 140 \pm 8 \text{ km s}^{-1}$) is not unusually large for O-type stars (Penny 1996; Howarth et al. 1997), and the star’s spin axis inclination, i_{spin} , would need to be relatively small if the star is currently a rapid rotator (see V_{eq} estimates in Table 5). We showed above that the star could have been a rapid rotator due to tidal interactions prior to the SN (see the $v_{\text{kick}}+$ solutions in Table 6). Nevertheless, we doubt that significant rotationally induced mixing has occurred since then because the elapsed time since the SN implied by the kinematical age ($< 1 \text{ My}$; Ribó et al. (2002)) is much smaller than the characteristic time for large scale mixing (comparable to the main sequence lifetime, $\approx 6 \text{ My}$; Heger & Langer (2000); Meynet & Maeder (2000)). Therefore, we doubt that the N-enrichment of LS 5039 is due to internal mixing unless the O-star was born as a rapid rotator and mixing has progressed for a long time (i.e., the lifetime of the neutron star progenitor plus the kinematical age).

The alternative explanation is that the nuclear processed gas was accreted from the SN progenitor. The system had a short orbital period prior to the SN explosion (Table 6) that probably resulted from a spiral-in during a common-envelope phase (CEP) (Taam & Sandquist 2000). The surviving O-star probably accreted relatively little material during the CEP because of its short duration, and accretion following the CEP must have been very limited because mass transfer at that point would have caused an expansion of the orbit (Hilditch 2001). Instead we suspect that the CNO-enriched gas was transferred from the progenitor during a period immediately prior to the start of the CEP. Massive donor

stars with radiative envelopes can in some circumstances sustain a stable mass transfer rate through Roche lobe overflow until the envelope is lost (Hjellming & Webbink 1987; Wellstein et al. 2001; Podsiadlowski et al. 2002), and it is possible that several solar masses of enriched gas were accreted by the O-star gainer during this evolutionary stage. Other explanations such as direct wind fed accretion (Clark et al. 2002) and accretion of the impacting SN shell (Fryxell & Arnett 1981) are less compelling because the amount of enriched gas accreted in both cases is relatively minor.

Many of the black hole MXRBs are also thought to have evolved from widely separated binaries into compact systems through a common envelope stage (Wellstein & Langer 1999; Podsiadlowski et al. 2003), and it is curious that these do not generally show the N enrichment we find in LS 5039. The explanation may be related to the youth of LS 5039 (Ribó et al. 2002). We suspect that thermohaline mixing (de Loore & Vanbeveren 1994), rotational mixing, and stellar wind mass loss will act to remove the enriched gas from the atmosphere so that the N enrichment may decline with the time elapsed since the SN. LS 5039 may represent an unusually young MXRB in which these processes have yet to make a significant change in the atmospheric abundances, so that the products of the intense binary interaction remain vividly intact in the stellar atmosphere.

We thank the staffs of CTIO, KPNO, and McDonald Observatory for their assistance in making these observations possible. We are especially grateful to Dr. Todd Henry and the SMARTS Consortium for the CTIO 1.5 m time awarded to this project. We also thank Dr. Thierry Lanz and Dr. Ivan Hubeny for the use of and advice about their codes *TLUSTY* and *Synspec*, Dr. Nolan Walborn for comments about the ON classification, Dr. Marc Ribó for communicating his radial velocity results in advance of publication, and the referee Dr. Philipp Podsiadlowski for his insights on binary evolution. PJW is grateful for continuing hospitality at the Department of Astrophysical Sciences, Princeton University. Support for this work (HST Proposal Number 9449) was provided by NASA through a grant from the Space Telescope Science Institute, which is operated by the Association of Universities for Research in Astronomy, Incorporated, under NASA contract NAS5-26555. Additional financial support was provided by the National Science Foundation through grant AST-0205297 (DRG). Institutional support has been provided from the GSU College of Arts and Sciences and from the Research Program Enhancement fund of the Board of Regents of the University System of Georgia, administered through the GSU Office of the Vice President for Research. This research made use of the Multimission Archive at the Space Telescope Science Institute (MAST), NASA’s Astrophysics Data System Bibliographic Service, and the Two Micron All Sky Survey, which is a joint project of the University of Massachusetts and the Infrared Processing and Analysis Center/California Institute of Technology, funded by NASA and

NSF.

REFERENCES

Berger, D. H., & Gies, D. R. 2001, *ApJ*, 555, 364

Bessell, M. S. 1983, *PASP*, 95, 480

Bhattacharya, D., & van den Heuvel, E. P. J. 1991, *Physics Rep.*, 203, 1

Bolton, C. T., & Rogers, G. L. 1978, *ApJ*, 222, 234

Brandt, N., & Podsiadlowski, Ph. 1995, *MNRAS*, 274, 461

Claret, A., & Cunha, N. C. S. 1997, *A&A*, 318, 187

Clark, J. S., et al. 2001, *A&A*, 376, 476

Clark, J. S., Goodwin, S. P., Crowther, P. A., Kaper, L., Fairbairn, M., Langer, N., & Brocksopp, C. 2002, *A&A*, 392, 909

Clausen, J. V., Larsen, S. S., Garcia, J. M., Giménez, A., & Storm, J. 1997, *A&AS*, 122, 559

Cousins, A. W. J. 1987, *South African Astron. Obs. Circ.*, 11, 93

Cutri, R. M., et al. 2003, The 2MASS All-Sky Catalog of Point Sources (Pasadena: Univ. Mass. & IPAC)

Dearborn, D. S. P. 1977, *ApLett*, 19, 15

De Greve, J. P., & de Loore, C. 1992, *A&AS*, 96, 653

de Loore, C., & Vanbeveren, D. 1994, *A&A*, 292, 463

Fitzpatrick, E. L. 1999, *PASP*, 111, 63

Fryxell, B. A., & Arnett, W. D. 1981, *ApJ*, 243, 994

Gies, D. R., Huang, W., & McSwain, M. V. 2002, *ApJ*, 578, L67

Gray, D. F. 1992, *The observation and analysis of stellar photospheres*, 2nd ed. (Cambridge: Cambridge Univ. Press)

Gray, R. O. 1998, *AJ*, 116, 482

Hatchett, S., & McCray, R. 1977, *ApJ*, 211, 552

He, L., Whittet, D. C. B., Kilkenny, D., & Spencer Jones, J. H. 1995, *ApJS*, 101, 335

Heger, A., & Langer, N. 2000, *ApJ*, 544, 1016

Henden, A. A., & Kaitchuck, R. H. 1982, *Astronomical Photometry* (New York: Van Nostrand Reinhold)

Hilditch, R. W. 2001, *An Introduction to Close Binary Stars* (Cambridge: Cambridge Univ. Press)

Hjellming, M. S., & Webbink, R. F. 1987, *ApJ*, 318, 794

Howarth, I. D., & Prinja, R. K. 1989, *ApJS*, 69, 527

Howarth, I. D., Siebert, K. W., Hussain, G. A. J., & Prinja, R. K. 1997, *MNRAS*, 284, 265

Howarth, I. D., & Smith, K. C. 2001, *MNRAS*, 327, 353

Hughes, A., & Bailes, M. 1999, *ApJ*, 522, 504

Kaper, L., Hammerschlag-Hensberge, G., & van Loon, J. Th. 1993, *A&A*, 279, 485

Kaper, L., Henrichs, H. F., Nichols, J. S., & Telting, J. H. 1999, *A&A*, 344, 231

Kilkenny, D. 1993, *South Afr. Astron. Obs. Circ.*, 15, 53

Kudritzki, R.-P., & Puls, J. 2000, *ARA&A*, 38, 613

Lamers, H. J. G. L. M., & Cassinelli, J. P. 1999, *Introduction to Stellar Winds* (Cambridge: Cambridge Univ. Press)

Lamers, H. J. G. L. M., van den Heuvel, E. P. J., & Petterson, J. A. 1976, *A&A*, 49, 327

Langer, N., Wellstein, S., & Petrovic, J. 2003, in *A Massive Star Odyssey, from Main Sequence to Supernova*, Proc. IAU Symp. 212, ed. K. A. van der Hucht, A. Herrero, & C. Esteban (San Francisco: A.S.P.), 275

Lanz, T., & Hubeny, I. 2003, *ApJS*, 146, 417

Martins, F., Schaerer, D., & Hillier, D. J. 2002, *A&A*, 382, 999

Mathys, G. 1989, *A&AS*, 81, 237

McSwain, M. V., & Gies, D. R. 2002, *ApJ*, 568, L27

McSwain, M. V., Gies, D. R., Riddle, R. L., Wang, Z., & Wingert, D. W. 2001, *ApJ*, 558, L43

Meynet, G., & Maeder, A. 2000, A&A, 361, 101

Morbey, C. L., & Brosterhus, E. B. 1974, PASP, 86, 455

Nelemans, G., Tauris, T. M., & van den Heuvel, E. P. J. 1999, A&A, 352, L87

Paredes, J. M., Martí, J., Ribó, M., & Massi, M. 2000, Science, 288, 2340

Paredes, J. M., Ribó, M., Ros, E., Martí, J., & Massi, M. 2002, A&A, 393, L99

Penny, L. R. 1996, ApJ, 463, 737

Pfahl, E., Rappaport, S., Podsiadlowski, Ph., & Spruit, H. 2002, ApJ, 574, 364

Podsiadlowski, Ph., Rappaport, S., & Han, Z. 2003, MNRAS, 341, 385

Podsiadlowski, Ph., Rappaport, S., & Pfahl, E. D. 2002, ApJ, 565, 1107

Prinja, R. K., Barlow, M. J., & Howarth, I. D. 1990, ApJ, 361, 607

Puls, J., et al. 1996, A&A, 305, 171

Reig, P., Ribó, M., Paredes, J. M., & Martí, J. 2003, A&A, 405, 285

Ribó, M., Paredes, J. M., Romero, G. E., Benaglia, P., Martí, J., Fors, O., & García-Sánchez, J. 2002, A&A, 384, 954

Ribó, M., Reig, P., Martí, J., & Paredes, J. M. 1999, A&A, 347, 518

Roberts, D. H., Lehár, J., & Dreher, J. W. 1987, AJ, 93, 968

Schönberner, D., Herrero, A., Becker, S., Eber, F., Butler, K., Kudritzki, R. P., & Simon, K. P. 1988, A&A, 197, 209

Stellingwerf, R. F. 1978, ApJ, 224, 953

Taam, R. E., & Sandquist, E. L. 2000, ARA&A, 38, 113

Vacca, W. D., Garmann, C. D., & Shull, J. M. 1996, ApJ, 460, 914

Vanbeveren, D., & de Loore, C. 1994, A&A, 290, 129

van den Heuvel, E. P. J., & van Paradijs, J. 1997, ApJ, 483, 399

van Loon, J. Th., Kaper, L., & Hammerschlag-Hensberge, G. 2001, A&A, 375, 498

Wade, R. A., & Rucinski, S. M. 1985, A&AS, 60, 471

Walborn, N. R. 1976, *ApJ*, 205, 416

Walborn, N. R., & Fitzpatrick, E. L. 1990, *PASP*, 102, 379

Walborn, N. R., Lennon, D. J., Heap, S. R., Lindler, D. J., Smith, L. J., Evans, C. J., & Parker, J. W. 2000, *PASP*, 112, 1243

Walborn, N. R., Nichols-Bohlin, J., & Panek, R. J. 1985, International Ultraviolet Explorer Atlas of O-Type Spectra from 1200 to 1900 Å (NASA RP-1155; Washington, DC: NASA)

Wellstein, S., & Langer, N. 1999, *A&A*, 350, 148

Wellstein, S., Langer, N., & Braun, H. 2001, *A&A*, 369, 939

Zahn, J.-P. 1977, *A&A*, 57, 383

Table 1. Spectrograph Parameters

UT Dates	Instrument	G/ λ_b /O ^a	Filter	CCD	$\lambda/\Delta\lambda$	Range (Å)
2002 Jun 07 ...	McD 2.7 m/LCS	1200/ 4000/1	...	TI	2500	4060–4770
2002 Jun 23–28	KPNO 0.9 m/CF	316/12000/2	OG550	TI	11630	6532–6708
2003 Mar 17 ...	CTIO 1.5 m/CS	831/ 8000/2	CuSO ₄	Loral	2320	4071–4741
2003 Mar 18–20	CTIO 1.5 m/CS	831/ 8000/2	BG39	Loral	2320	4071–4741
2003 Mar 21 ...	CTIO 1.5 m/CS	831/ 8000/1	GG495	Loral	1800	5488–6799
2003 Apr 26 ...	McD 2.7 m/LCS	1200/ 4000/1	...	Loral	2500	4071–4790
2003 Apr 27–28	McD 2.7 m/LCS	1200/ 4000/1	...	TI	2500	4056–4764

^aGrating grooves mm⁻¹/ blaze wavelength (Å)/ order.

Table 2. New Radial Velocities

HJD (2450000+)	Orbital Phase	V_r (km s $^{-1}$)	$O - C$ (km s $^{-1}$)	Source
2432.902 ..	0.901	-17.8	-4.0	McD blue
2448.858 ..	0.505	12.5	8.3	KPNO red
2449.839 ..	0.727	-3.6	2.7	KPNO red
2450.811 ..	0.946	-11.7	-0.6	KPNO red
2453.801 ..	0.622	5.9	7.1	KPNO red
2715.894 ..	0.829	-10.3	1.3	CTIO blue
2716.902 ..	0.057	17.1	-1.4	CTIO blue
2717.901 ..	0.282	17.0	2.6	CTIO blue
2718.839 ..	0.495	9.5	4.9	CTIO blue
2719.881 ..	0.730	-17.2	-10.7	CTIO red
2755.901 ..	0.867	-9.9	3.3	McD blue
2756.849 ..	0.081	28.6	7.8	McD blue
2756.957 ..	0.106	31.7	10.3	McD blue
2757.956 ..	0.331	6.9	-5.2	McD blue

Note. — See McSwain et al. (2001) for earlier measurements that were used in the orbital solution.

Table 3. Orbital Elements

Element	Value
P (d)	4.4267 ± 0.0005
T (HJD - 2,450,000)	2756.49 ± 0.07
K (km s $^{-1}$)	17.6 ± 1.3
V_0 (km s $^{-1}$)	4.1 ± 0.8
e	0.48 ± 0.06
ω (deg)	268 ± 10
rms (km s $^{-1}$)	5.5
$f(m)$ (M_\odot)	0.0017 ± 0.0005
$a_1 \sin i$ (R_\odot)	1.36 ± 0.12

Table 4. He Line Ratios and Effective Temperature

Ratio	$\log[W_\lambda(\text{He II}) / W_\lambda(\text{He I})]$	T_{eff} (kK)
He II $\lambda 4541$: He I $\lambda 4471$	0.29 ± 0.02	37.9 ± 0.4
He II $\lambda 4541$: He I $\lambda 4387$	0.68 ± 0.03	35.4 ± 0.4
He II $\lambda 4200$: He I $\lambda 4144$	1.00 ± 0.05	36.3 ± 0.3
He II $\lambda 4200$: He I $\lambda 4713$	0.86 ± 0.03	39.8 ± 0.3

Table 5. Range in Stellar Parameters

Parameter	$M_O = 20M_\odot$	$M_O = 30M_\odot$	$M_O = 40M_\odot$
$R_O (R_\odot)$	7.0	8.5	9.9
v_∞/v_{esc}	2.5	2.2	2.1
$\log \dot{M} (M_\odot \text{ y}^{-1})^a$	−7.5	−7.4	−7.3
$\log \dot{M} (M_\odot \text{ y}^{-1})^b$	−7.0	−6.8	−6.6
$M_X (M_\odot)$	1.3	1.4	1.5
R_O (Roche) (R_\odot) ^c	10.0	11.9	13.3
d (kpc)	1.9	2.4	2.7
V_{eq} (km s ^{−1}) ^d	198	168	149

^aFrom H α for the 2000 October minimum, the time of the KPNO Coude Feed (McSwain & Gies 2002) and BeppoSAX observations (Reig et al. 2003).

^bBased on the wind momentum relationship for Galactic O-type stars of luminosity classes III and V (Kudritzki & Puls 2000).

^cMean Roche radius of the O star at periastron.

^dFrom $V \sin i$ and $i_{\text{spin}} = i_{\text{orbit}}$.

Table 6. Pre-Supernova Orbital Parameters

Parameter	v_{kick}	$M_O = 20M_\odot$	$M_O = 30M_\odot$	$M_O = 40M_\odot$
P^{initial} (d)	0	1.39	1.39	1.39
M_2^{initial} (M_\odot)	0	11.6	16.6	21.5
v_{sys} (predicted) (km s^{-1})	0	181	210	233
v_{pec} (derived) (km s^{-1})	95	118	137
$\langle P^{\text{initial}} \rangle$ (d)	+	1.52	1.58	1.63
M_2^{initial} (M_\odot)	+	6.9	10.4	14.5
$\langle v_{\text{kick}} \rangle$ (km s^{-1})	+	58	51	41
$\langle \nu \rangle$ (deg)	+	3	2	1
$\langle V_{\text{sync}} \rangle$ (km s^{-1})	+	232	273	306
$\langle P^{\text{initial}} \rangle$ (d)	-	4.61	4.60	4.81
M_2^{initial} (M_\odot)	-	7.4	11.5	16.0
$\langle v_{\text{kick}} \rangle$ (km s^{-1})	-	182	211	226
$\langle \nu \rangle$ (deg)	-	13	12	11
$\langle V_{\text{sync}} \rangle$ (km s^{-1})	-	77	94	104

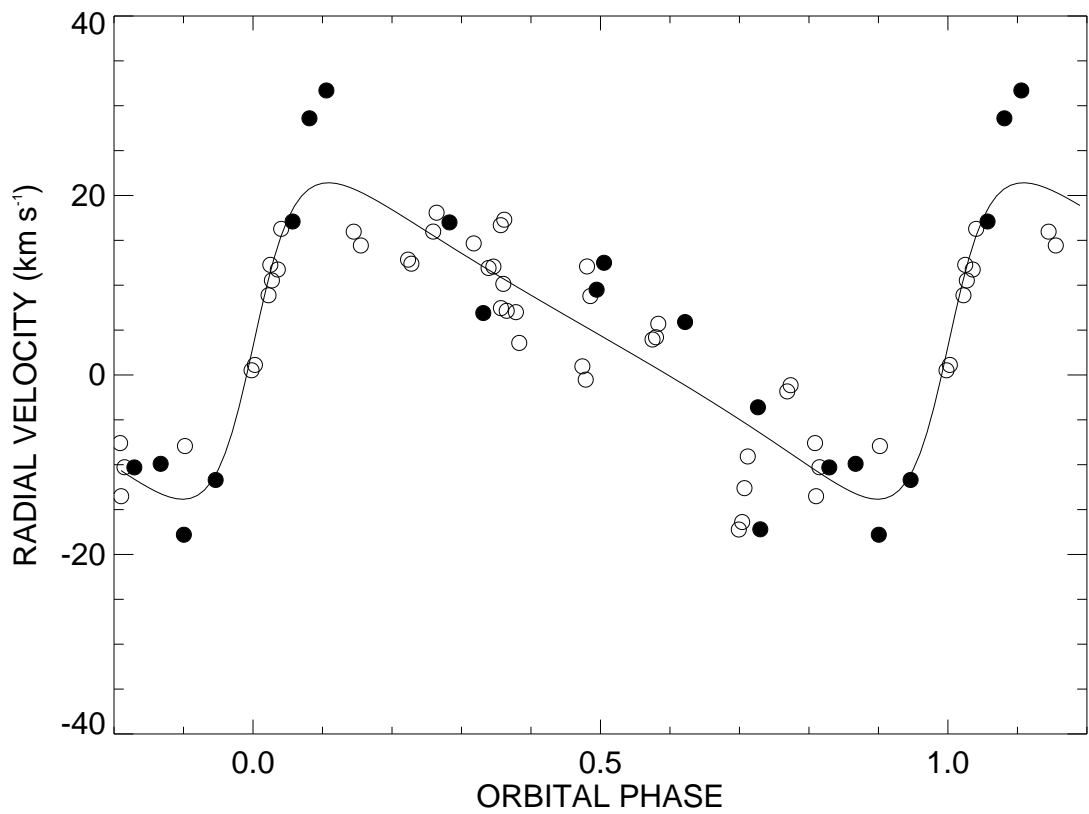


Fig. 1.— The revised radial velocity curve (*solid line*) for LS 5039 together with the original measurements from McSwain et al. (2001) (*open circles*) and the new measurements (*filled circles*).

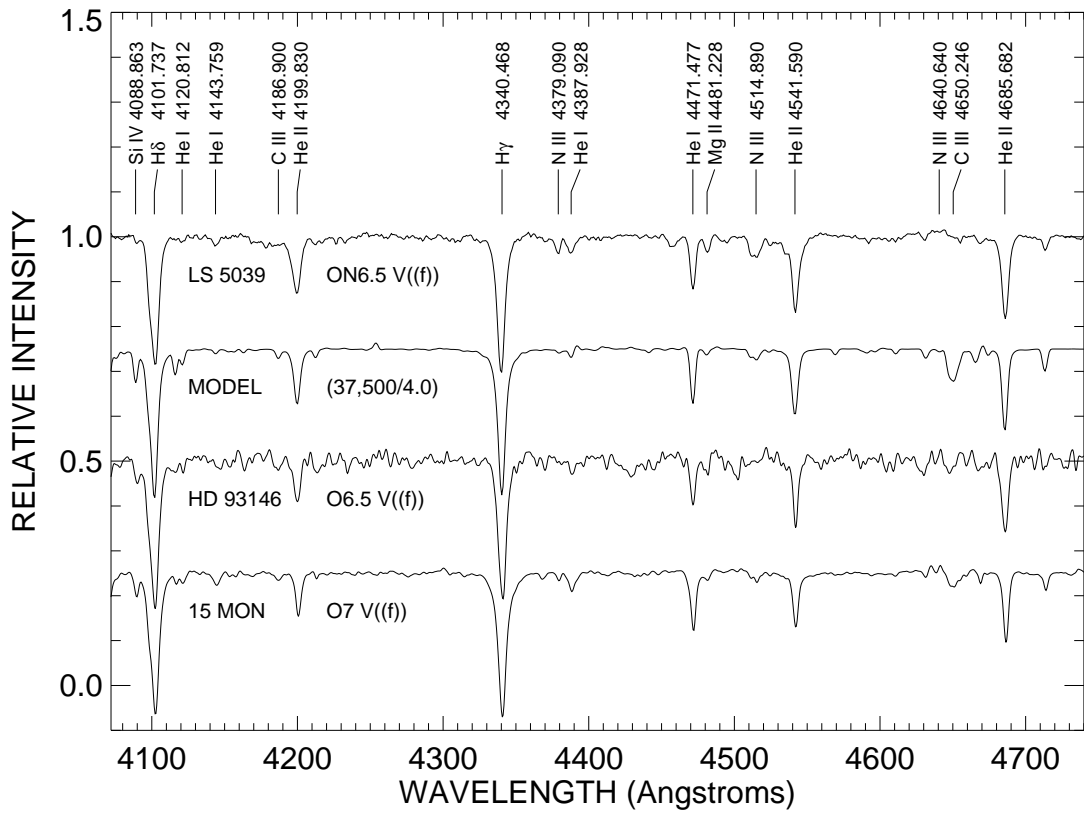


Fig. 2.— The average spectrum of LS 5039 compared to the model spectrum from Lanz & Hubeny (2003), an O6.5 V((f)) standard from Walborn & Fitzpatrick (1990), and an O7 V((f)) standard (from our CTIO run). Some of the stronger lines are identified at the top. The lines of N III are systematically stronger (and the C III lines weaker) in the spectrum of LS 5039 than in the other spectra.

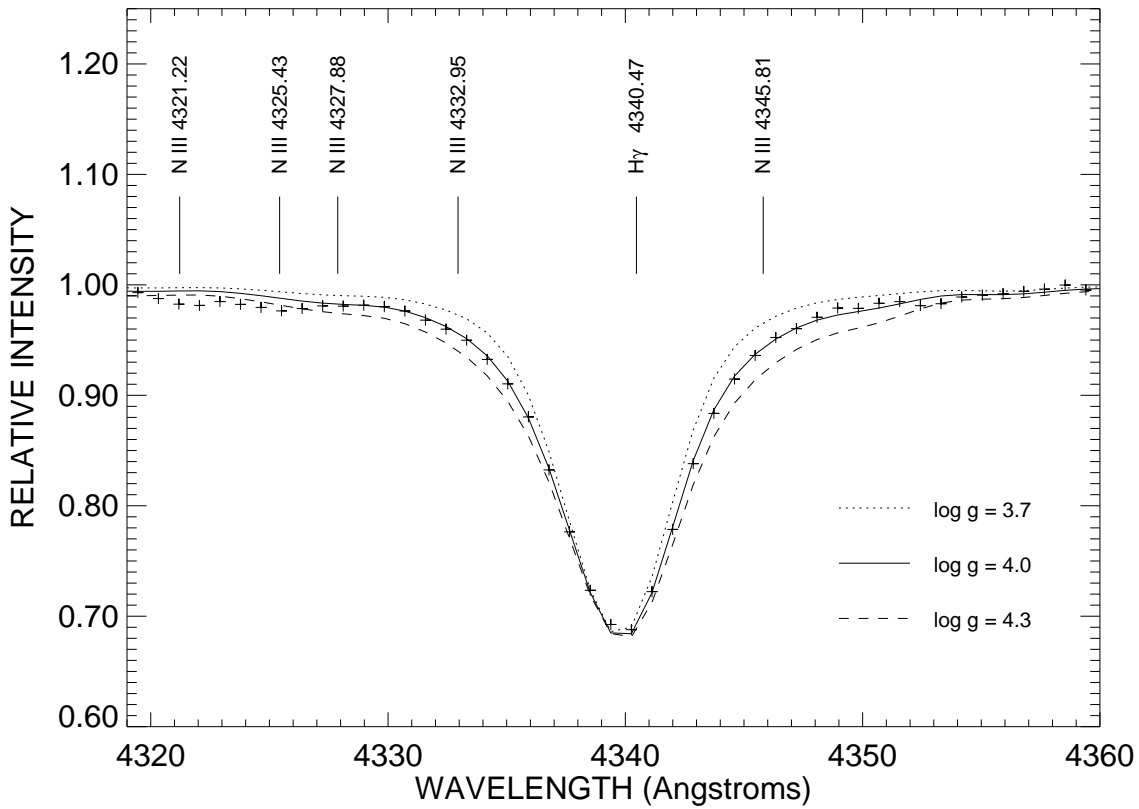


Fig. 3.— The $H\gamma$ profile in the average spectrum of LS 5039 (*plus signs*) compared to the model profiles from Lanz & Hubeny (2003) for three values of atmospheric gravity (and corresponding pressure broadening of the Balmer line wings). Possible line blends from transitions of N III are identified above.

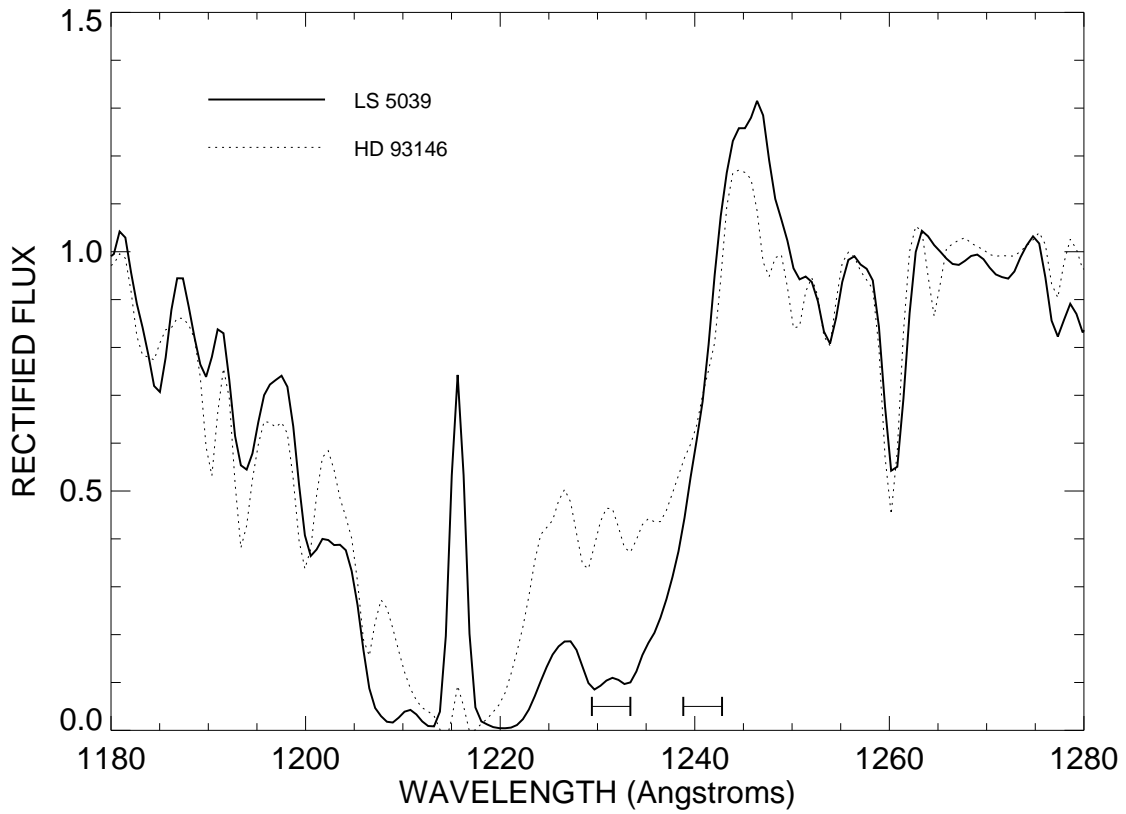


Fig. 4.— The N V $\lambda\lambda 1238.821, 1242.804$ P Cygni profile in the spectrum of LS 5039 (*solid line*) compared to that of the O6.5 V((f)) standard star, HD 93146 (*dotted line*). The error bars at the bottom show the rest wavelengths of the doublet (*right*) and the Doppler shifted wavelengths of the narrow absorption components (*left*). The strong emission feature at 1216 Å is geocoronal Ly α .

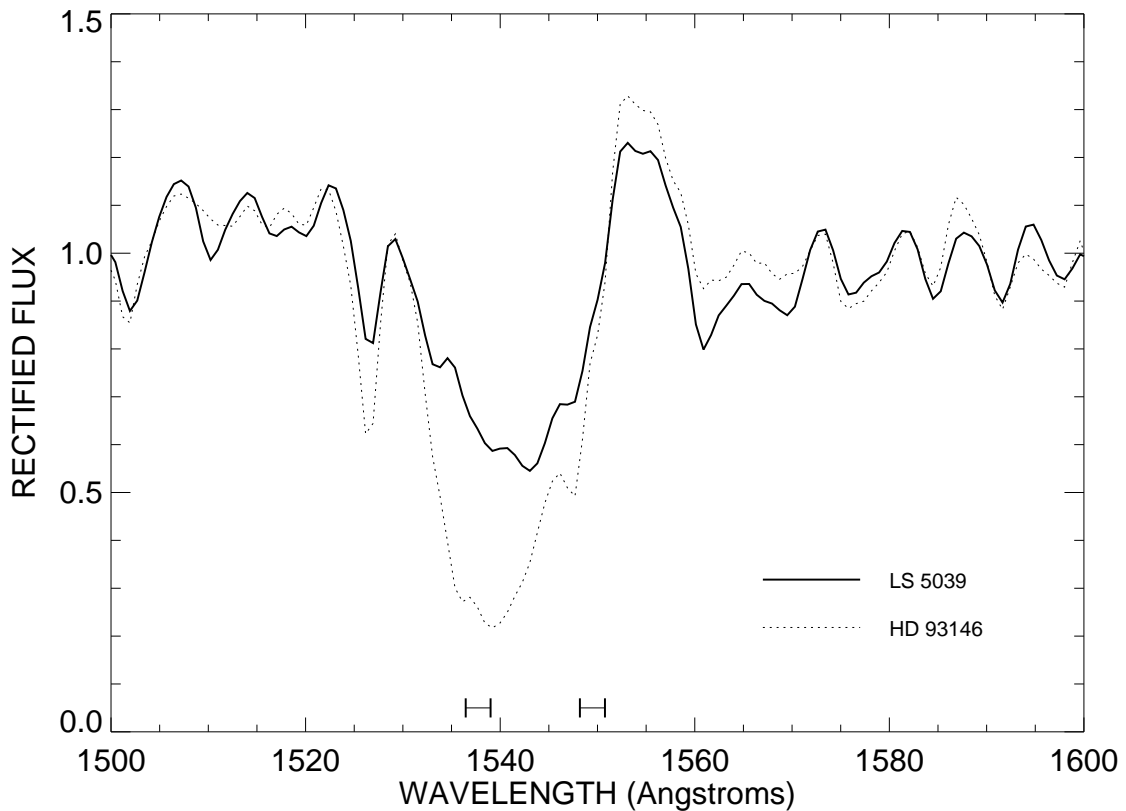


Fig. 5.— The C IV $\lambda\lambda 1548.195, 1550.770$ P Cygni profile in the spectrum of LS 5039 (*solid line*) compared to that of the O6.5 V((f)) standard star, HD 93146 (*dotted line*). The error bars at the bottom show the rest wavelengths of the doublet (*right*) and the Doppler shifted wavelengths of the narrow absorption components (*left*).

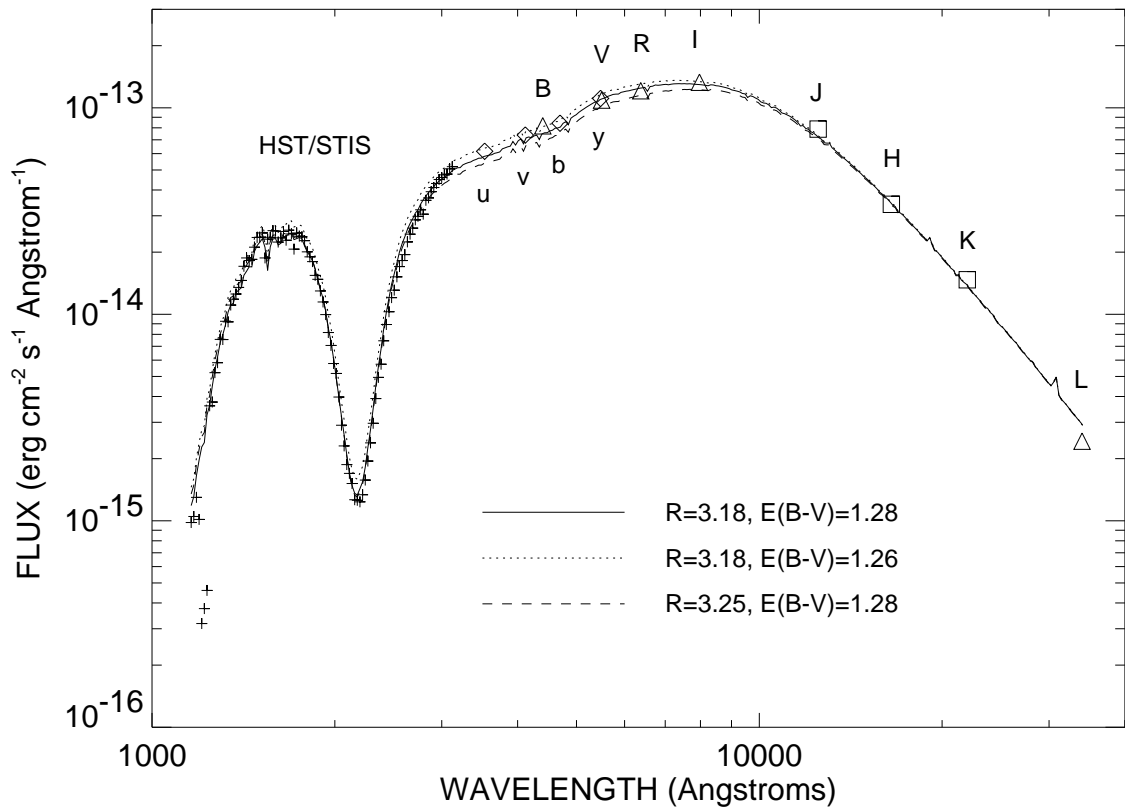


Fig. 6.— The UV, optical, and IR flux distribution of LS 5039 compared to model flux distributions for several assumptions about the ratio of total to selective extinction, R , and reddening, $E(B-V)$. The data sources include UV fluxes from *HST/STIS* (plus signs), CTIO Strömgren photometry (diamonds), Johnson B , V , Cousins R , I , and IR L -band photometry from Clark et al. (2001) (triangles), and IR J , H , K photometry from the 2MASS survey (Cutri et al. 2003) (squares).

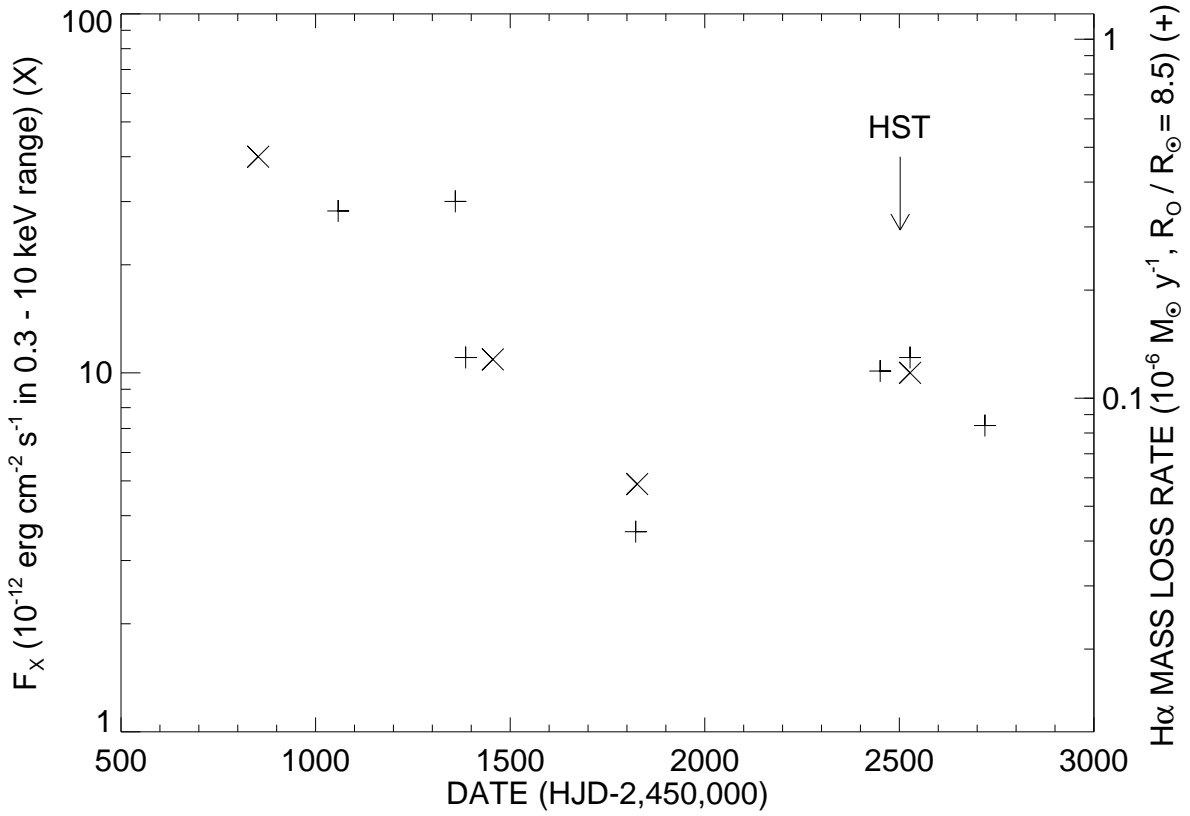


Fig. 7.— The co-variability of the observed X-ray flux in the 0.3 – 10 keV range (Reig et al. 2003) (X marks) and $H\alpha$ mass loss rate (+ signs) as a function of time. The mass loss rate was determined assuming a stellar radius of $R_O/R_\odot = 8.5$, which corresponds to a mass of $M_O/M_\odot = 30$. The date of the HST/STIS observation is indicated by an arrow.

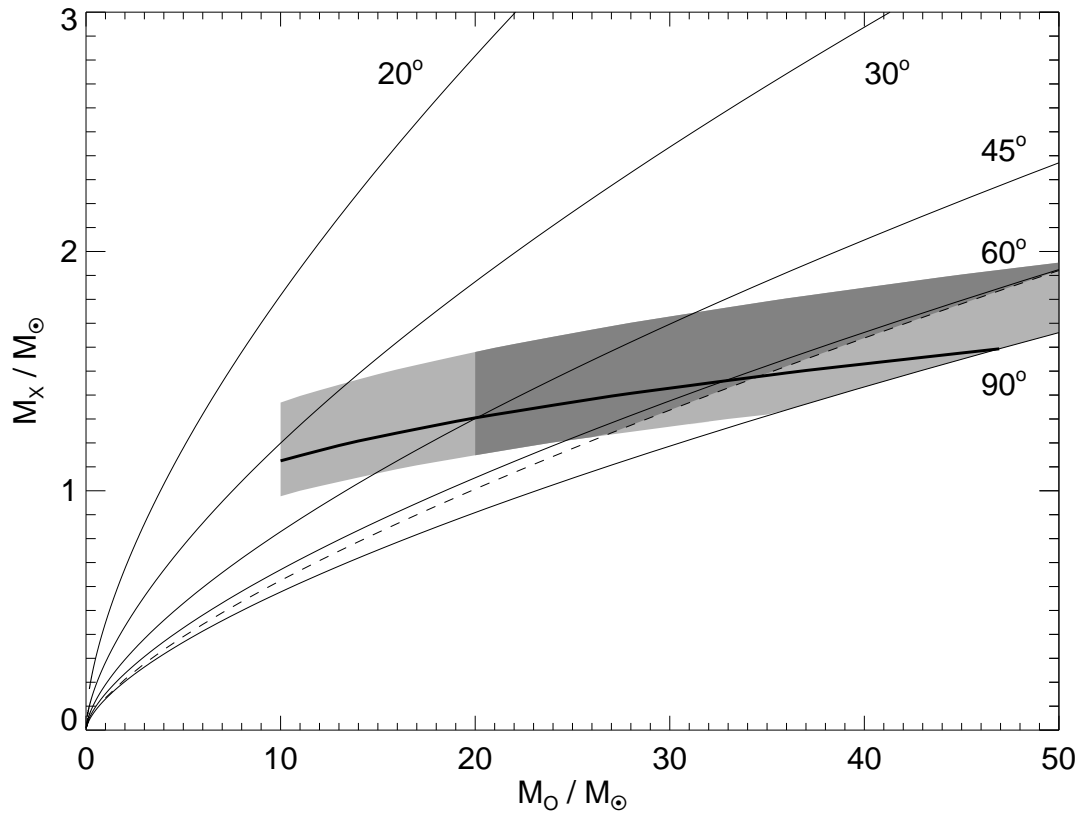


Fig. 8.— A mass plane diagram for LS 5039 with constraints from the wind accretion model. The thin solid lines trace the mass solutions from the orbital elements for the labelled values of orbital inclination. The thick solid line shows the mass relationship derived by matching the observed and predicted X-ray fluxes from the wind accretion model (with the lightly shaded region showing possible solutions found by adjusting parameters discussed in the text). The dashed line indicates the lower limit on M_X established by the lack of observed eclipses, and the darker shaded region shows the most probable mass solution space.

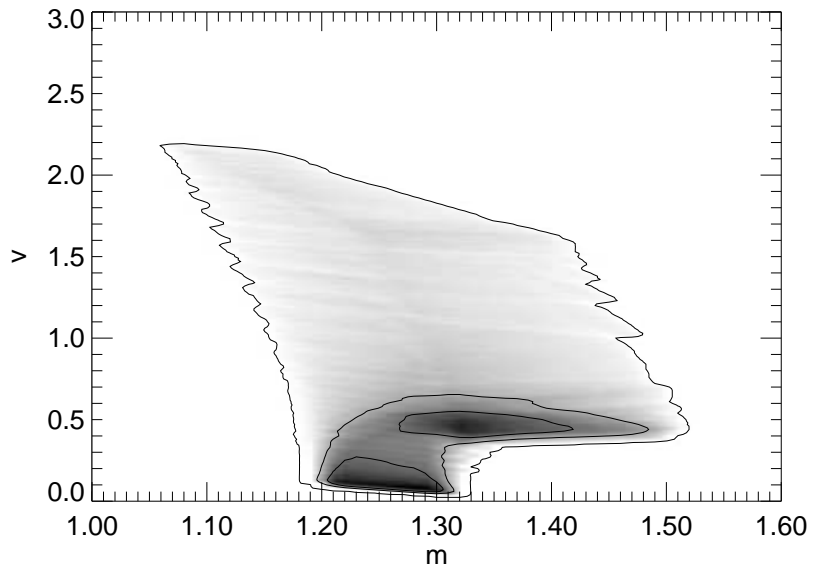


Fig. 9.— A grayscale representation of the solution space of supernova mass loss parameters (assuming $M_O = 30M_\odot$ and $M_X = 1.4M_\odot$; the corresponding plots for the $M_O = 20$ and $40M_\odot$ cases look similar except for small shifts in m). The gray intensity indicates the fraction of solid angle into which a kick velocity is directed that results in an eccentricity and space velocity equal within errors to the derived values. Contour lines are shown for acceptable solutions in 10, 5, and 0.1% of the solid angle sphere (the darkest, maximum value corresponds to 20%). The solutions are parameterized by m , the ratio of total binary mass before to that after the supernova, and v , the ratio of the kick velocity to the initial relative orbital velocity (Brandt & Podsiadlowski 1995).